Scientific
Research

Adsorption Enthalpy Calculations of Hydrogen Adsorption at Ambient Temperature and Pressures Exceeding 300 bar

Matthew Beckner[1], Anne Dailly[2]

[1]Optimal CAE Inc., Plymouth, USA
[2]Chemical and Materials Systems Laboratory, General Motors Global Research and
Development Center, Warren, USA
Email: matthew.beckner@gm.com

ABSTRACT

Hydrogen adsorption isotherms were measured at ambient temperature to pressures exceeding 300 bar for three benchmark adsorbents: two metal-organic frameworks, $Cu_3(btc)_2$ (btc = 1,3,5-benzenetricarboxylate) and $Zn_4O(btb)_2$ (btb = 1,3,5-benzenetribenzoate), and the activated carbon MSC-30. The Dubinin-Astakhov model was applied to calculated absolute adsorption isotherms as a function of the fugacity to determine the adsorption enthalpy at ambient temperature. Comparisons of the calculated enthalpies and the surface excess concentration (excess adsorption per square meter of surface) show that $Zn_4O(btb)_2$ has an adsorption enthalpy comparable to MSC-30, but that the spacing between adsorbed molecules is much larger.

Keywords: Ambient Temperature Hydrogen Storage; Metal-Organic Frameworks; Activated Carbon; Adsorption Enthalpy

1. Introduction

One major challenge hindering the use of hydrogen in on-board vehicular applications is overcoming the low volumetric energy density of hydrogen at ambient conditions (0.0107 MJ/L) [1]. In order to match the energy density of gasoline (31.1 MJ/L) [1], hydrogen at ambient temperature must be compressed to a pressure greater than 5 kbar. While this pressure is extremely impractical for vehicular applications, prototype fuel cell vehicles do operate at pressures up to 700 bar. The use of high-pressure compressed hydrogen requires relatively expensive and large, cylindrical tanks that occupy a significant amount of cargo space [2,3]. An alternative approach to achieve a high-energy density is to use high specific surface area materials in which hydrogen is reversibly adsorbed on the surface without any chemical change or bonding [4]. Research into these materials has focused on increasing the specific surface area, optimizing pore geometry, and increasing the adsorption energy. In particular, the adsorption energy for most materials is between 4 and 7 kJ/mol [5]. Numerical estimations have shown that an adsorption energy between 12 and 20 kJ/mol will be necessary for ambient temperature operating conditions [5,6].

There are several pathways to increase the adsorption energy in microporous materials. One is by changing the width of the pore to create an overlapping adsorption potential. This is achieved by adjusting the activation parameters in activated carbons [7] or by adjusting the length of the linker in metal-organic frameworks (MOFs) [8]. The adsorption energy can also be increased by creating inhomogeneous charge distributions in the adsorbent surface. In metal-organic frameworks (MOFs), focus has been given to producing partially coordinated secondary building units (SBU) [5,9,10] while work in carbonaceous materials has focused on the use of heavy or light metal doping [6,11,12].

Regardless of the method used to make materials with higher adsorption energies, it is necessary to experimentally verify the adsorption energy. The adsorption energy may be measured directly using calorimetry, but the most common method is the so-called isosteric method. The isosteric method employs a form of the van't Hoff equation [13,14]

$$\Delta \dot{h}_{ads} = R \left(\frac{\partial \ln [p]}{\partial \left(\frac{1}{T} \right)} \right)_\theta \qquad (1)$$

to measure the adsorption enthalpy $\Delta \dot{h}_{ads}$ and involves measuring several adsorption isotherms at different temperatures. Lines of constant surface coverage θ (isosteres) are graphed as $\ln[p]$ vs. $\frac{1}{T}$.

In this paper, we use experimental data at ambient temperature and high-pressure for three benchmark materials to calculate the adsorption enthalpy. We show that careful consideration must be taken before applying Equation (1) to high-pressure data, and that a single isotherm can be used if an appropriate adsorption model is selected. Additionally, we show that volumetric storage for these benchmark materials is only a marginal improvement, at best, over compressed hydrogen and that excess adsorption must be increased to improve storage capacity.

2. Materials

Three benchmark adsorbent materials were used for this study. MSC-30 is an activated carbon produced from petroleum coke by Kansai Coke and Chemicals Co. Zn_4O $(1,3,5\text{-benzenetribenzoate})_2$ ($Zn_4O(btb)_2$; MOF-177) is a MOF consisting of tetragonal $[Zn_4O]^{6+}$ SBUs connected by tricarboxylate ligands. This sample of $Zn_4O(btb)_2$ was synthesized at pilot scale by BASF as Basolite Z377. $Cu_3(1,3,5\text{-benzenetricarboxylate})_2$ ($Cu_3(btc)_2$; HKUST-1) is a MOF with copper paddlewheel SBUs connected by btc ligands. In contrast to $Zn_4O(btb)_2$, $Cu_3(btc)_2$ has open metal sites. $Cu_3(btc)_2$ is commercialized by Sigma-Aldrich as Basolite C300. All MOFs were stored in an argon glove box. All samples were degassed at 120°C for 12 hours prior to adsorption measurements.

3. Materials Porosity Characterization

Subcritical argon isotherms were measured using an Autosorb-1 (Quantachrome Instruments). Brunauer-Emmett-Teller (BET) surface areas were measured using the pressure range of 0.03 - 0.1 P/P$_0$. The measured surface areas of the MOF samples (**Table 1**) were similar to previously measured values [5], indicating that the material porosity was well activated and the remaining solvent was completely removed. The specific pore volume v_{pore} was measured at 0.995 P/P$_0$ by assuming liquid density within the pores. The specific pore volume includes only void volume within individual grains and

does include any intergranular void space.

Using the specific pore volume and the measured skeletal density ρ_s, the void fraction ϕ was calculated using the following equation [7]

$$\phi \equiv \frac{V_{pore}}{V_{pore} + V_{solid}} = \left(1 + \left(\rho_s v_{pore}\right)^{-1}\right)^{-1} \quad (2)$$

where V_{pore} is the total volume of pores for a given volume of adsorbent V_{solid}. Micropore volumes were determined using the Dubinin–Radushkevich (DR) method. Pore size distributions (PSD) were calculated using the nonlocal density function method. For $Zn_4O(btb)_2$ and $Cu_3(btc)_2$, it was assumed that the samples contained both cylindrical and spherical pores. MSC-30 was assumed to have slit shaped pores. PSDs for the materials are shown in **Figure 1**. All of the pores in $Cu_3(btc)_2$ are less than 12 Å due to the short btc ligand. The larger btb ligand used in $Zn_4O(btb)_2$ resulted in wider pores.

The activated carbon, MSC-30, has a PSD that is indicative of chemical activation in which metallic potassium from KOH, the activating agent, intercalates between graphitic sheets, causing micropore formation [7,15]. The larger (>12 Å) pores are formed by dehydration of KOH to K_2O which reacts with CO_2 to form potassium carbonate. Washing of the carbon after activation removes the intercalated potassium, potassium carbonate, and other residual products to leave the observed pore structure.
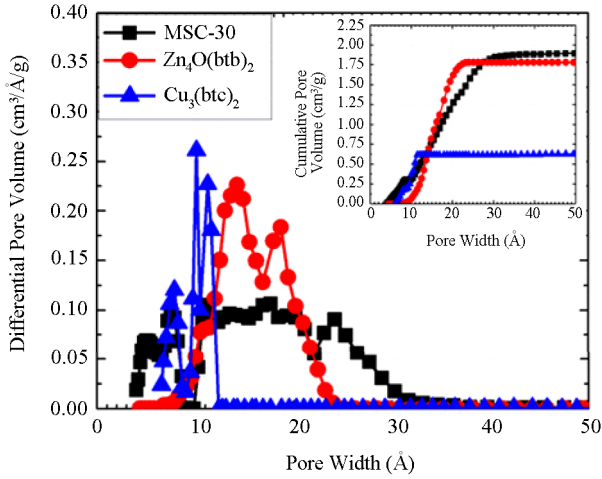
4. Hydrogen Adsorption Data

Hydrogen isotherms were measured at room temperature up to 320 bar using a custom-built volumetric adsorption instrument described previously [16,17]. Helium deadspace measurements were completed to determine sample skeletal density ρ_s (**Table 2**). It was assumed that the effects of helium adsorption were negligible. All hydrogen densities $\rho_{H_2}(p,T)$ used for isotherm calculations were determining using the NIST REFPROP database (version 8.0).

Hydrogen excess adsorption isotherms are shown in **Figure 2** top. The gravimetric storage m_{st} [g H$_2$/g Sample] and volumetric storage v_{st} [g H$_2$/L Sample] were calculated from the excess adsorption isotherms m_{exc} [g H$_2$/g Sample] assuming a granular packing fraction of

Table 1. Summary of sample characteristics calculated from argon isotherms.

Sample	BET Surface Area (m²/g)	Specific Pore Volume (g/cm³)	DR Micro-pore Volume (g/cm³)	Void Fraction
MSC-30	3400	2.14	1.89	0.82
Zn$_4$O(btb)$_2$	4100	1.67	0.51	0.73
Cu$_3$(btc)$_2$	1300	0.57	0.35	0.49

Figure 1. Differential pore volumes and cumulative pore volumes (inset) calculated from subcritical argon adsorption isotherms using non-local density functional theory for MSC-30 (black squares), Zn$_4$O(btb)$_2$ (red circles), and Cu$_3$(btc)$_2$ (blue triangles).

unity (*i.e.* disregarding gas stored between individual adsorbent grains). The gravimetric storage was therefore calculated using

$$m_{st} = m_{exc} + \rho_{H_2}(p,T)v_{pore} \tag{3}$$

and the volumetric storage was calculated using

$$v_{st} = m_{st}\rho_{app} \tag{4}$$

where ρ_{app} is the apparent density of the adsorbent. The apparent density is

$$\rho_{app} \equiv \frac{m_s}{V_{solid} + V_{pore}} = \rho_s(1-\phi) \tag{5}$$

and

$$v_{st} = m_{st}\rho_s(1-\phi) \tag{6}$$

Alternatively, in terms of excess adsorption,

$$v_{st} = \left(m_{exc} + \rho_{H_2}(p,T)v_{pore}\right)\rho_s(1-\phi) \tag{7}$$

$$v_{st} = \left(m_{exc} + \frac{\rho_{H_2}(p,T)}{\rho_s}\frac{\phi}{1-\phi}\right)\rho_s(1-\phi) \tag{8}$$

and

$$v_{st} = m_{exc}\rho_s(1-\phi) + \rho_{H_2}(p,T)\phi \tag{9}$$

Because Equation (3) does not include gas stored between powder grains, Equation (3) represents the theoretical minimum for the value of m_{st} in a real tank.

In order for a material to store more hydrogen volumetrically than a compressed hydrogen tank, the excess adsorption must be greater than the amount of gas that would be present in the volume occupied by the adsorbent. In other words, it must be true that

$$m_{exc} > \frac{V_{solid}}{m_s}\rho_{H_2}(p,T) = \frac{\rho_{H_2}(p,T)}{\rho_s} \tag{10}$$

which is readily obtained from Equation (9). If the Inequality (10) is true, then including the intergranular space will decrease the volumetric storage capacity. However, if instead $m_{exc} < \rho_{H_2}/\rho_s$, then including the intergranular space will actually increase the volumetric storage capacity. In order to improve adsorbent systems over compressed hydrogen, it is paramount to increase the excess adsorption to as high a value as possible.
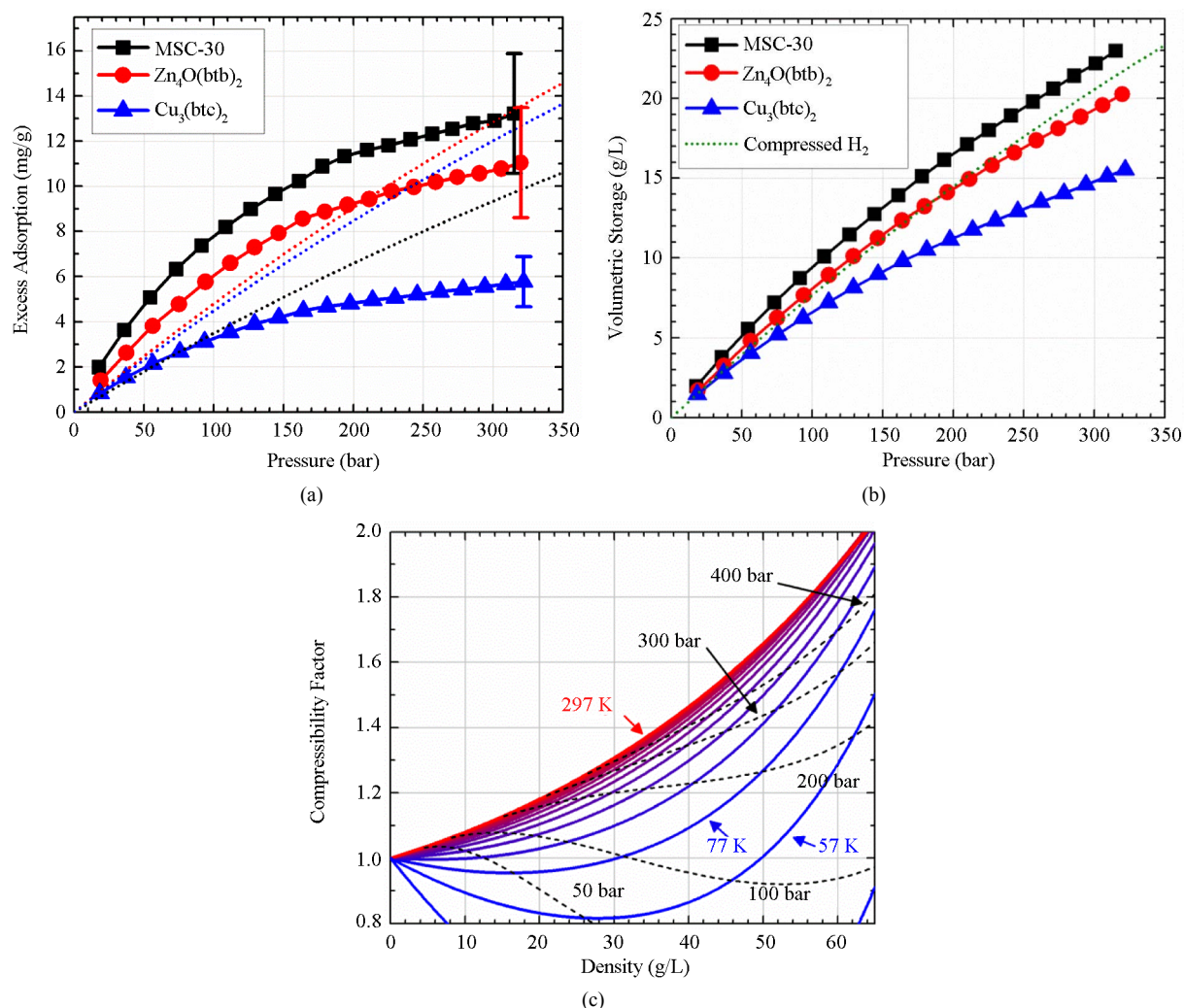
The volumetric storage capacities calculated from Equation (6) are shown in **Figure 2(b)**. Only MSC-30 and Zn$_4$O(btb)$_2$ have volumetric storage capacities that exceed compressed hydrogen. At ambient temperature, hydrogen adsorption is relatively small effect. This is demonstrated in **Figure 2(a)** which shows that the difference between the excess adsorption and the right hand side of Inequality (10) is very small. For example, the ratio of the left-hand side of Inequality (10) to the right-hand side for Zn$_4$O(btb)$_2$ at 75 bar is ~1.4. By sharp contrast, the same ratio for Zn$_4$O(btb)$_2$ measured at 77 K and 65 bar from [5] is ~5.2.

The large difference between 77 K and ambient temperature adsorption can be explained by examining the interactions in the adsorption system. In an adsorption system, the presence of an interaction between the surface and the gas creates a condensed gaseous film on the surface. The amount of compression at a given pressure will be balanced by the intermolecular repulsion of the gas so that the spacing of molecules on the surface is limited by the natural repulsion between gas molecules.

One way of quantifying this compressibility is by defining a compressibility factor

Table 2. Summary of helium and hydrogen adsorption measurements.

Sample	Skeletal Density (g/cm^3)	Sample Mass Used for H$_2$ Ads. (g)	Temperature of H$_2$ Measurement (K)	H$_2$ Excess Ads. at ~320 bar (mg/g)
MSC-30	2.2 ± 0.1	0.543	295.2	13 ± 2
Zn$_4$O(btb)$_2$	1.6 ± 0.1	0.488	298.2	11 ± 2
Cu$_3$(btc)$_2$	1.71 ± 0.03	1.037	296.1	6 ± 1

Figure 2. (a) hydrogen excess adsorption at ambient temperature for all materials measured graphed with ρ_{H_2}/ρ_s (dotted lines). (b) volumetric storage at ambient temperature for all materials measured. The green dotted line indicates the density of hydrogen. (c) the compressibility of hydrogen in 20 K increments. The black lines indicate isobars.

$$z \equiv \frac{p}{\rho RT} \qquad (11)$$

which is related to the virial coefficients $B_i(T)$ by

$$z = 1 + \sum_{i=2}^{\infty} B_i(T)\rho^{i-1} \qquad (12)$$

By Equation (12), the compressibility factor is directly related to the repulsive and attractive interactions of the gas. The gas is non-interacting (ideal) for $z = 1$. If $z < 1$, then most interactions between gas molecules are attractive. If $z > 1$, then most interactions between gas molecules are repulsive. As shown in **Figure 2(c)**, the compressibility factor is a smaller value at 77 K than at 297 K. This means that it is takes less energy to compress hydrogen into a denser state at low temperatures compared to room temperature. Therefore, the adsorption energy must be increased to overcome this extra repul-

sive energy.

5. Enthalpy Calculations

5.1. Surface Excess Concentration

One method of evaluating the strength of the adsorbent-gas interaction is by calculating the surface excess concentration Γ (SEC) from excess adsorption using

$$\Gamma = \frac{m_{exc}}{\Sigma} \qquad (13)$$

where Σ is the BET surface area. The SEC is a measure of how closely spaced the adsorbed molecules are on the adsorbent's surface and it is a good qualitative assessment of the adsorption energy. For microporous materials, the BET surface area can depend greatly upon the adsorbate used, because the measurable surface area is limited by the adsorbate's molecular size.

When comparing SECs calculated for different adsorbents, the BET surface areas should be measured using the same adsorbate.

Calculated SECs for the three materials investigated are shown in **Figure 3(a)**. Although $Cu_3(btc)_2$ has the lowest excess adsorption, it also has the highest SEC. For the $Zn_4O(btb)_2$, the adsorbed hydrogen molecules are not as closely spaced indicating that either it has a relatively low binding energy or that only some of the available surface area contributes to the hydrogen adsorption. Because the SEC is only a qualitative assessment of the adsorption energy, the actual adsorption enthalpy, Equation (1), must be calculated to quantify the behavior exhibited in the SEC.

5.2. Non-Ideality Corrections

Equation (1) is derived for an ideal gas. However, at higher pressure, deviations from ideal gas behavior can be significant. For instance, the difference in density between ideal gas hydrogen and real hydrogen at 300 bar and 296 K is nearly 20%. Noting that, for an ideal gas, the fugacity f is equivalent to the pressure, Equation (1) may be applied to a real gas by substituting the fugacity in place of the ideal gas pressure [18,19]

$$\Delta \dot{h}_{ads}^{(real)} = R \left(\frac{\partial \ln [f]}{\partial \left(\frac{1}{T} \right)} \right)_{\theta} \tag{14}$$

or in terms of the fugacity coefficient φ and the real gas pressure p_{exp}

$$\Delta \dot{h}_{ads}^{(real)} = R \left(\frac{\partial \ln \left[p_{exp} \varphi \right]}{\partial \left(\frac{1}{T} \right)} \right)_{\theta} \tag{15}$$

It follows that the natural logarithm may be split into two parts

$$\Delta \dot{h}_{ads}^{(real)} = R \left(\frac{\partial \ln \left[p_{exp} \right]}{\partial \left(\frac{1}{T} \right)} \right)_{\theta} + R \left(\frac{\partial \ln [\varphi]}{\partial \left(\frac{1}{T} \right)} \right)_{\theta} \tag{16}$$

$$\Delta \dot{h}_{abs}^{(real)} = \Delta \dot{h}_{abs}^{(exp)} + \Delta \dot{h}_{abs}^{(cor)} \tag{17}$$

where the enthalpy $\Delta \dot{h}_{ads}^{(exp)}$ is Equation (14) assuming that the real gas is an ideal gas and the correction enthalpy $\Delta \dot{h}_{ads}^{(cor)}$ is an additional term that is a function of the fugacity coefficient and temperature. The correction enthalpy is the difference between using the experimental data as a function of the fugacity and using it as a function of the pressure.

The correction enthalpy may be calculated using fugacity coefficients determined using an appropriate equation of state (EOS) [20]. The fugacity coefficients as a function of temperature and pressure were calculated using an empirically derived EOS for hydrogen given by [21]. As shown in **Figure 3(b)**, near ambient temperature, the correction to the ideal gas equation is small (<0.1 kJ/mol). It is not until low temperature and high pressure that the correction becomes significant. This is extremely important because if the real pressure is used without

(a)

(b)
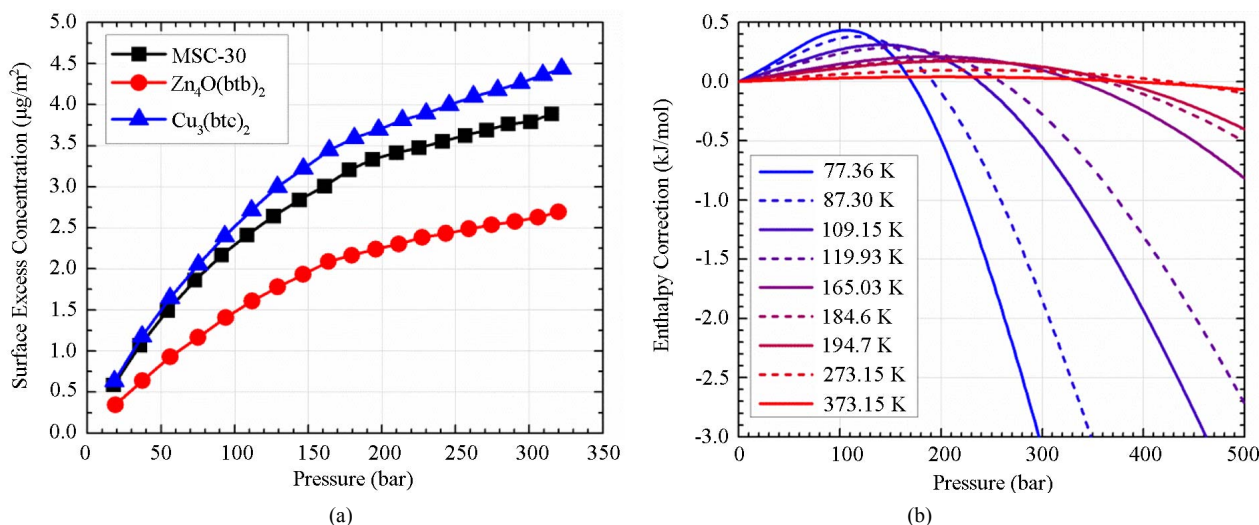
Figure 3. (a) surface excess concentration for all materials measured indicating the packing density of adsorbed molecules on the surface and (b) the correction to the adsorption enthalpy $\left(\Delta \dot{h}_{ads}^{(cor)} \right)$ required to account for non-ideality of hydrogen. The temperatures shown here are the normal boiling points of several gases (from lowest to highest temperature): N_2, Ar, CH_4, Kr, Xe, C_2H_6, CO_2 (sublimation), H_2O (melting point), and H_2O (boiling point).

correcting for the gas's non-ideality, any calculated enthalpy will be overestimated at high pressure.

It is an important distinction that Equation (14) can apply to either excess adsorption or absolute adsorption, but the two are not thermodynamically equivalent. At low temperature and pressure, where excess and absolute adsorptions are approximately equal, the two enthalpies are also approximately equal. However, as Mertens described [22], at high pressure or temperature the difference can lead to huge discrepancies. Adsorption enthalpies calculated from excess adsorption should be referred to as "isoexcess" enthalpies to avoid confusion [23]. Since measured adsorption isotherms are given in terms of excess adsorption, absolute adsorption must be calculated before using Equation (14).

5.3. Absolute Adsorption

Excess adsorption is defined in terms of the total mass of hydrogen in the system per mass of adsorbent m, the hydrogen density, the volume available to the hydrogen per mass of adsorbent v_0

$$m_{\text{exc}} = m - \rho_{\text{H}_2}(p,T) v_0 \qquad (18)$$

If one excludes all molecules that are at the density $\rho_{\text{H}_2}(p,T)$, then Equation (18) is instead

$$m_{\text{exc}} = m_{\text{abs}} - \rho_{\text{H}_2}(p,T) v_{\text{ads}} \qquad (19)$$

and

$$m_{\text{abs}} = m_{\text{exc}} + \rho_{\text{H}_2}(p,T) v_{\text{ads}} \qquad (20)$$

Here, v_{ads} is the volume occupied by the adsorbed film per mass of adsorbent ($v_{\text{ads}} \leq v_{\text{pore}}$)

Numerous ways of determining v_{ads} have been suggested [24-27]. We have chosen here to use the specific pore volume v_{pore} as measured by subcritical argon isotherms. Assuming that the volume accessible to argon is equal to the volume accessible to hydrogen, then v_{pore} represents the largest possible value of v_{ads} and it gives the upper limit to the possible values of the absolute adsorption. When calculated in this way, the absolute adsorption is equivalent to the gravimetric storage.

5.4. The Dubinin-Astakhov Model

Before Equation (14) may be applied to the calculated absolute adsorption, the data must be fit with a temperature dependent adsorption model. Here we use the Dubinin-Astakhov (DA) model of micropore filling. The model has been described previously [13,14,28], but we summarize it here. The DA model for absolute adsorption is given by

$$w = w_0 \exp\left[-\left(\frac{A}{E}\right)^{\xi}\right] \qquad (21)$$

where w is the volume of hydrogen adsorbed, w_0 is the micropore volume, E is a temperature and pressure independent characteristic energy of the gas-adsorbent system, A is the adsorption potential, and ξ is a structural heterogeneity factor [28]. The adsorption potential A is given by [14,28]

$$A = RT \ln\left[\frac{f_s}{f}\right] \qquad (22)$$

where f_s is the fugacity at saturation. For supercritical adsorption, such as hydrogen at ambient temperature, the saturation fugacity is ill-defined. A pseudo-saturation fugacity must be defined, such as was suggested by Amankwah and Schwarz [28],

$$f_s = \left(\frac{T}{T_c}\right)^{\gamma} p_c \qquad (23)$$

where T_c and p_c are the critical temperature and pressure respectively and the parameter γ is an empirical constant particular to the adsorbate-adsorbent system. The final form of the DA model is

$$w = w_0 \exp\left[-\left(\frac{RT \ln\left[\left(\frac{T}{T_c}\right)^{\gamma}\left(\frac{p_c}{f}\right)\right]}{E}\right)^{\xi}\right] \qquad (24)$$

w/w_0 a unitless quantity representing the fraction of pore volume filled. Because it is a unitless quantity, it is equivalent to represent the micropore filling as ratio of the mass adsorbed m_{abs} to the mass adsorbed at complete saturation m_0 so that Equation (24) is

$$m_{\text{abs}} = m_0 \exp\left[-\left(\frac{RT \ln\left[\left(\frac{T}{T_c}\right)^{\gamma}\left(\frac{p_c}{f}\right)\right]}{E}\right)^{\xi}\right] \qquad (25)$$

By solving Equation (25) for the fugacity and applying Equation (14), the adsorption enthalpy is given by

$$\Delta \dot{h}_{\text{ads}} = E \ln\left[\frac{m_0}{m_{\text{abs}}}\right]^{\frac{1}{\xi}} + \gamma RT \qquad (26)$$

Equation (24) depends upon the temperature of the isotherm measured. The zero temperature enthalpy $\Delta \dot{h}_{\text{ads}}(T=0)$ is a useful quantity, because it represents the change in energy of the gas upon adsorption.

One note about the DA model is that, at low pressure, it does not satisfy Henry's law. This is further exemplified in Equation (26). For small values of m_{abs}, the cal-

culated enthalpy goes toward infinity, meaning that the model loses physical meaning at low coverage. This method is only accurate for application to high pressure adsorption of supercritical gases or to multilayer subcritical adsorption.

For the samples studied, the order from highest to lowest enthalpy (**Figure 4(a)**) does not match the order of the SEC from highest to lowest. From **Figure 3(a)**, it is clear that the adsorbed molecules as not spaced as closely in $Zn_4O(btb)_2$ as the other samples, but the adsorption enthalpy is comparable to MSC-30. The best conclusion to make from this is that not all of the available surface area is contributing to adsorption at this temperature, but the portion that does contribute has an interaction that is comparable to activated carbon. The adsorption enthalpy for $Cu_3(btc)_2$ is larger than $Zn_4O(btb)_2$ which is consistent with the idea that MOFs with open (exposed) metal sites will have a higher adsorption energy. The zero temperature enthalpy (**Figure 4(b)**) and the characteristic energy (**Table 3**) show values that are expected of the materials investigated. The activated carbon, MSC-30, has a $\Delta \dot{h}_0$ at low coverage of about 5 kJ/mol. Although the adsorption enthalpy for $Cu_3(btc)_2$ does exceed 12 kJ/mol at low coverage, almost half of this enthalpy is due to temperature effects. Additionally, the enthalpy quickly decreases with increasing

pressure. A storage material that will be potentially useful for vehicular applications at ambient temperature operating conditions will require an enthalpy that is above 12 kJ/mol for the entire pressure range.

6. Conclusions

For the three benchmark materials measured, volumetric storage at ambient temperature is only a marginal improvement, at best, over compressed hydrogen. This is because hydrogen adsorption at ambient temperature is a relatively small effect and the difference between excess adsorption and gas that could be stored in the volume that the material displaces is small. Excess adsorption must therefore be increased to improve storage capacity.

The fugacity must be used in place of the real gas pressure when calculating adsorption enthalpies. Use of the experimental pressure can result in large errors in the calculated enthalpy at high pressure. The DA model may be used for high-pressure, ambient temperature adsorption data to calculate the adsorption enthalpy from a single adsorption isotherm. Finally, the surface excess concentration has been shown to be a good qualitative measurement for the adsorption enthalpy because high enthalpy materials tend to have more closely spaced adsorbed molecules. However, it is not a perfect metric, as
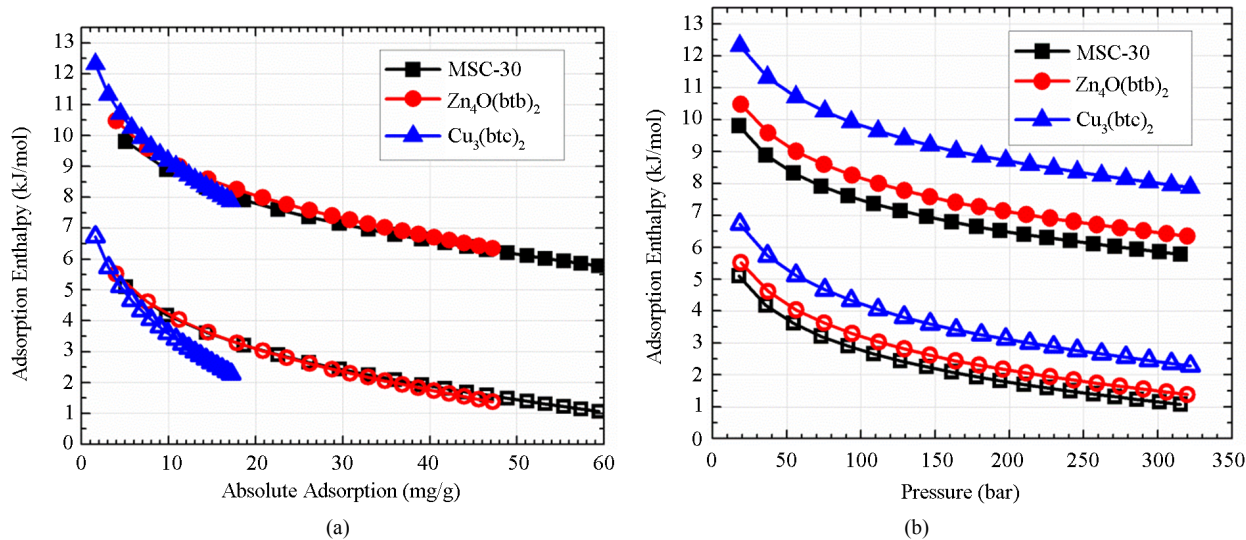
Figure 4. The adsorption enthalpy (solid symbols) and zero temperature adsorption enthalpy (open symbols) calculated from the DA equation as a function of absolute adsorption (a) and pressure (b).

Table 3. Fitting parameters obtained for the DA model.

Sample	m_0 [mg/g]	E [kJ/mol]	γ	ξ
MSC-30	83.5	4.41	1.92	1.35
$Zn_4O(btb)_2$	69.5	4.74	2.00	1.44
$Cu_3(btc)_2$	28.9	5.85	2.26	1.60

　　AJAC

shown for $Zn_4O(btb)_2$, if a portion of the surface area is not contributing to the adsorption process.

7. Acknowledgments

REFERENCES

[1]   G. Thomas, "Overview of Storage Development DOE Hydrogen Program," 2000. http://www1.eere.energy.gov/hydrogenandfuelcells/pdfs/storage.pdf

[2]   U. Eberle, B. Müller and R. von Helmolt, "Fuel Cell Electric Vehicles and Hydrogen Infrastructure: Status 2012," *Energy & Environmental Science*, Vol. 5, No. 10, 2012, pp. 8780-8798. http://dx.doi.org/10.1039/c2ee22596d

[3]   "How FCX Clarity FCEV Works," 2013. http://automobiles.honda.com/fcx-clarity/how-fcx-works.aspx

[4]   J. Burress, M. Kraus, M. Beckner, R. Cepel, G. Suppes, C. Wexler and P. Pfeifer, "Hydrogen Storage in Engineered Carbon Nanospaces," *Nanotechnology*, Vol. 20, No. 20, 2009, Article ID: 204026. http://dx.doi.org/10.1088/0957-4484/20/20/204026

[5]   L. J. Murray, M. Dincă and J. R. Long, "Hydrogen Storage in Metal-organic Frameworks," *Chemical Society Reviews*, Vol. 38, No. 5, 2009, pp. 1294-1314. http://dx.doi.org/10.1039/b802256a

[6]   L. Firlej, S. Roszak, B. Kuchta, P. Pfeifer and C. Wexler, "Enhanced Hydrogen Adsorption in Boron Substituted Carbon Nanospaces," *Journal of Chemical Physics*, Vol. 131, No. 16, 2009, Article ID:164702. http://dx.doi.org/10.1063/1.3251788

[7]   J. Romanos, M. Beckner, T. Rash, L. Firlej, B. Kuchta, P. Yu, G. Suppes, C. Wexler and P. Pfeifer, "Nanospace Engineering of KOH Activated Carbon," *Nanotechnology*, Vol. 23, No. 1, 2012, Article ID: 015401. http://dx.doi.org/10.1088/0957-4484/23/1/015401

[8]   H. Deng, S. Grunder, K. E. Cordova, C. Valente, H. Furukawa, M. Hmadeh, F. Gándara, A. C. Whalley, Z. Liu, S. Asahina, H. Kazumori, M. O'Keeffe, O. Terasaki, J. F. Stoddart and O. M. Yaghi, "Large-Pore Apertures in a Series of Metal-Organic Frameworks," *Science*, Vol. 336, No. 6084, 2012, pp. 1018-1023. http://dx.doi.org/10.1126/science.1220131

[9]   D. J. Collins and H.-C. Zhou, "Hydrogen Storage in Metal-Organic Frameworks," *Journal of Materials Chemistry*, Vol. 17, No. 30, 2007, pp. 3154-3160. http://dx.doi.org/10.1039/b702858j

[10] M. Dincă, A. Dailly, Y. Liu, C. M. Brown, D. A. Neumann and J. R. Long, "Hydrogen Storage in a Microporous Metal-Organic Framework with Exposed Mn^{2+} Coordination Sites," *Journal of the American Chemical Society*, Vol. 128, No. 51, 2006, pp. 16876-16883.

http://dx.doi.org/10.1021/ja0656853

[11] Y. Ferro, F. Marinelli, A. Allouche and C. Brosset, "Density Functional Theory Investigation of H Adsorption on the Basal Plane of Boron-Doped Graphite," *The Journal of Chemical Physics*, Vol. 118, No. 12, 2003, pp. 5650-5657. http://dx.doi.org/10.1063/1.1556091

[12] T. C. M. Chung, Y. Jeong, Q. Chen, A. Kleinhammes and Y. Wu, "Synthesis of Microporous Boron-Substituted Carbon (b/c) Materials Using Polymeric Precursors for Hydrogen Physisorption," *Journal of the American Chemical Society*, Vol. 130, No. 21, 2008, pp. 6668-6669. http://dx.doi.org/10.1021/ja800071y

[13] F. Rouquerol, J. Rouquerol and K. Sing, "Adsorption by Powders & Porous Solids," Academic Press, London, 1999.

[14] E. Poirier, R. Chahine, P. Bénard, L. Lafi, G. Dorval-Douville and P. A. Chandonia, "Hydrogen Adsorption Measurements and Modeling on Metal-Organic frameworks and Single-Walled Carbon Nanotubes," *Langmuir*, Vol. 22, No. 21, 2006, pp. 8784-8789. http://dx.doi.org/10.1021/la061149c

[15] T. Otowa, R. Tanibata and M. Itoh, "Production and Adsorption Characteristics of MAXSORB: High-Surface-Area Active Carbon," *Gas Separation & Purification*, Vol. 7, No. 4, 1993, pp. 241-245. http://dx.doi.org/10.1016/0950-4214(93)80024-Q

[16] T. Voskuilen, Y. Zheng and T. Pourpoint, "Development of a Sievert Apparatus for Characterization of High Pressure Hydrogen Sorption Materials," *International Journal of Hydrogen Energy*, Vol. 35, No. 19, 2010, pp. 10387-10395. http://dx.doi.org/10.1016/j.ijhydene.2010.07.169

[17] T. G. Voskuilen, T. L. Pourpoint and A. M. Dailly, "Hydrogen Adsorption on Microporous Materials at Ambient Temperatures and Pressures up to 50 MPa," *Adsorption*, Vol. 18, No. 3-4, 2012, pp. 239-249. http://dx.doi.org/10.1007/s10450-012-9397-z

[18] A. M. Tolmachev, "Adsorption of Gases, Vapors, and Solutions: II. Description and a Priori Calculations of Adsorption Equilibria," *Protection of Metals and Physical Chemistry of Surfaces*, Vol. 46, No. 3, 2010, pp. 291-308.

[19] A. L. Myers, "Thermodynamics of Adsorption in Porous Materials," *AIChE Journal*, Vol. 48, No. 1, 2002, pp. 145-160. http://dx.doi.org/10.1002/aic.690480115

[20] E. W. Lemmon and R. T. Jacobsen, "A New Functional Form and New Fitting Techniques for Equations of State with Application to Pentafluoroethane (HFC-125)," *Journal of Physical and Chemical Reference Data*, Vol. 34, No. 1, 2005, pp. 69-108. http://dx.doi.org/10.1063/1.1797813

[21] J. W. Leachman, R. T. Jacobsen, S. G. Penoncello and E. W. Lemmon, "Fundamental Equations of State for Para-hydrogen, Normal Hydrogen, and Orthohydrogen," *Journal of Physical and Chemical Reference Data*, Vol. 38, No. 3, 2009, pp. 721-748. http://dx.doi.org/10.1063/1.3160306

[22] F. O. Mertens, "Determination of Absolute Adsorption in Highly Ordered Porous Media," *Surface Science*, Vol.

603, No. 10-12, 2009, pp. 1979-1984.
http://dx.doi.org/10.1016/j.susc.2008.10.054

[23] S. Sircar, "Gibbsian Surface Excess for Gas Adsorption Revisited," *Industrial & Engineering Chemistry Research*, Vol. 38, No. 10, 1999, pp. 3670-3682.
http://dx.doi.org/10.1021/ie9900871

[24] G. Aranovich and M. Donohue, "Determining Surface Areas from Linear Adsorption Isotherms at Supercritical Conditions," *Journal of Colloid and Interface Science*, Vol. 194, No. 2, 1997, pp. 392-397.
http://dx.doi.org/10.1006/jcis.1997.5099

[25] D. Saha, Z. Wei and S. Deng, "Equilibrium, Kinetics and Enthalpy of Hydrogen Adsorption in MOF-177," *International Journal of Hydrogen Energy*, Vol. 33, No. 24, 2008, pp. 7479-7488.
http://dx.doi.org/10.1016/j.ijhydene.2008.09.053

[26] N. P. Stadie, M. Murialdo, C. C. Ahn and B. Fultz, "Anomalous Isosteric Enthalpy of Adsorption of Methane on Zeolite-templated Carbon," *Journal of the American Chemical Society*, Vol. 135, No. 3, 2013, pp. 990-993.
http://dx.doi.org/10.1021/ja311415m

[27] E. Poirier and A. Dailly, "Thermodynamics of Hydrogen Adsorption in MOF-177 at Low Temperatures: Measurements and Modelling," *Nanotechnology*, Vol. 20, No. 20, 2009, Article ID: 204006.
http://dx.doi.org/10.1088/0957-4484/20/20/204006

[28] K. A. G. Amankwah and J. A. Schwarz, "A Modified Approach for Estimating Pseudo-Vapor Pressures in the Application of the Dubinin-Astakhov Equation," *Carbon*, Vol. 33, No. 9, 1995, pp. 1313-1319.
http://dx.doi.org/10.1016/0008-6223(95)00079-S